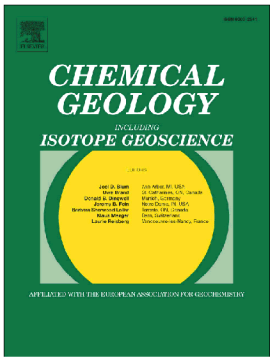

The distribution of neodymium isotopes and concentrations in the eastern tropical North Atlantic

Moritz Zieringer, Martin Frank, Roland Stumpf, Ed C. Hathorne

PII: S0009-2541(18)30584-9
DOI: https://doi.org/10.1016/j.chemgeo.2018.11.024
Reference: CHEMGE 18986

To appear in: *Chemical Geology*

Received date: 12 April 2018
Revised date: 9 October 2018
Accepted date: 28 November 2018

Please cite this article as: Moritz Zieringer, Martin Frank, Roland Stumpf, Ed C. Hathorne , The distribution of neodymium isotopes and concentrations in the eastern tropical North Atlantic. Chemge (2018), https://doi.org/10.1016/j.chemgeo.2018.11.024

The distribution of neodymium isotopes and concentrations in the eastern tropical North Atlantic

Moritz Zieringer, Martin Frank, Roland Stumpf, Ed C. Hathorne

GEOMAR Helmholtz Centre for Ocean Research Kiel, Wischhofstraße 1-3, 24148 Kiel, Germany

corresponding author:

Moritz Zieringer, GEOMAR Helmholtz Centre for Ocean Research Kiel, Wischhofstraße 1-3, 24148 Kiel, Germany, phone +49 431 600 2242, E-mail: mzieringer@geomar.de

Abstract:

Dissolved neodymium (Nd) and its radiogenic isotope composition ($^{143}Nd/^{144}Nd$, expressed as εNd) belong to the key parameters of the international GEOTRACES program, which aims to investigate the processes controlling the distribution of trace elements and their isotopes in the global ocean. We present Nd isotope and concentration ([Nd]) data from eleven full depth water column profiles from the eastern (sub)tropical Atlantic Ocean between 2°N and 29°N and from the Romanche Fracture Zone sampled during Meteor cruise M81/1 (GEOTRACES cruise GA11) in February/March 2010.

The εNd signatures range from -12.9 in upper North Atlantic Deep Water (UNADW) at the equator to -8.1 in the mixed layer near the Canary Islands. Nd concentrations range from 11.9 pmol/kg observed within the Equatorial Undercurrent to 40.2 pmol/kg in Antarctic Bottom Water (AABW) in the Romanche Fracture Zone. Large variations in surface water Nd

isotope compositions (-12.7 ≤ εNd ≤ -8.1) and concentrations (15.7 pmol/kg ≤ [Nd] ≤ 27.7 pmol/kg) are caused by partial dissolution of Saharan dust particles between 2°N and 13°N and volcanic island weathering (Canaries) between 25°N and 29°N. In contrast to dust inputs, which predominantly affect the Nd concentrations and isotope compositions of surface waters and underlying South Atlantic Central Water (SACW), contributions originating from the Canary Islands affect the Nd isotope composition of the entire surrounding water column without significantly altering Nd concentrations, thus confirming the concept of boundary exchange in its strictest sense.

The results confirm that the composition of lower North Atlantic Deep Water (LNADW, εNd= -12.1) in the abyssal plains of the eastern North Atlantic is exclusively set by the mixing ratio of LNADW and Antarctic Bottom Water (AABW). Upper North Atlantic Deep Water (UNADW), in contrast, is characterized by εNd signatures between -12.7 and -12.0 between 2°N and 10°N, whereas further north it is clearly affected by admixture of Mediterranean Water (MW) and radiogenic inputs from the Canary Islands and likely also the Cape Verde Islands.

Keywords: Neodymium isotopes, neodymium concentrations, eastern North Atlantic, GEOTRACES GA11, North Atlantic circulation

1. Introduction

1.1 Neodymium in seawater

The radiogenic isotope composition of dissolved Nd ($^{143}Nd/^{144}Nd$ expressed in εNd values) in seawater provides valuable information about the provenance of water masses, their flow paths and their present and past mixing (e.g. Piepgras and Wasserburg, 1987; Jeandel et al., 1993; Tachikawa et al., 1999; Lacan and Jeandel, 2004; 2005; Rickli et al., 2009; 2010; Stichel et al., 2012; 2015; Garcia-Solsona et al., 2014; Howe et al., 2016; Lambelet et al., 2016). Dissolved Nd in seawater is of lithogenic origin and water masses are labeled with specific Nd isotope compositions through exchange processes at the ocean margins. Its applicability as a source tracer is thus based on the heterogenous distribution of εNd signatures in continental rocks. ^{143}Nd is a decay product of ^{147}Sm and thus the radiogenic Nd isotope composition of a geological formation is primarily a function of lithology and age (cf. Frank, 2002). With Sm being relatively enriched in the mantle, εNd is less radiogenic (lower) in the Earth's crust than in the mantle and therefore oceanic basins predominantly surrounded by old cratonic rocks, like the Atlantic Ocean, have a lower mean εNd value than basins primarily surrounded by mantle-derived rocks (Piepgras and Wasserburg, 1980). With an oceanic residence time that is close to or shorter than the 1500 year time scale of global ocean mixing (Tachikawa et al., 1999; Arsouze et al., 2009 and Rempfer et al., 2011) and the independence of radiogenic Nd isotopes from biological fractionation (e.g. Bayon et al., 2016) Nd isotopes have been successfully applied as a quasi-conservative circulation tracer in the deep open ocean where mixing with other water masses is the prevailing cause for a change in εNd. In contrast, at the ocean margins processes like eolian or fluvial input (e.g. Goldstein et al., 1984; Albarède and Goldstein, 1992; Grasse et al., 2012, 2017), submarine groundwater discharge (e.g. Johannesson and Burdige, 2007; Molina-Kescher et al., 2018), or boundary exchange processes (Lacan and Jeandel, 2005), which may include a substantial pore water

flux (Haley et al., 2018), can strongly modify the local Nd budget. The relative importance of sources or exchange fluxes is poorly constrained but such knowledge is vital for understanding the modern Nd budget and to improve the application of Nd isotopes as a water mass tracer in the present and past ocean. Nd isotopes and REE concentrations are key parameters of the international GEOTRACES program, which aims to identify and quantify the processes that supply and remove trace elements (including Nd) and their isotopes (TEIs), as well as the physical and biological processes that redistribute TEIs within and between ocean basins.

Within the Atlantic Ocean major intermediate and deep water masses can clearly be discriminated on the basis of εNd signatures (Piepgras and Wasserburg, 1987). North Atlantic Deep Water in the western basin of the mid-latitude Atlantic is characterized by an εNd value between -13.2 ± 1.0 and -12.4 ± 0.4 (Lambelet et al. 2016). In contrast, Antarctic Intermediate Water (AAIW) and Antarctic Bottom Water (AABW), which sandwich the NADW, have a more radiogenic (less negative) εNd signature ranging between -9.5 and -7.9 in the Atlantic sector of the Southern Ocean (Stichel et al. 2012). Under the swift circulation regime of the western Atlantic basin this leads to close co-variations of Nd isotopes with salinity (von Blanckenburg, 1999) reflecting the suitability of Nd isotopes to be used as a water mass tracer. However, in marked contrast to the western basin, previous results have shown that the correspondence between water masses and εNd signatures is less clear in the eastern Atlantic basin, at least between the Strait of Gibraltar and the Cape Verde Islands (Stichel et al., 2015).

Here we present full water column Nd isotope and concentration data from the eastern tropical North Atlantic (ETNA) between the equator and the Canary Islands including the first data between the Cape Verde Islands and the equator. Our study aims to elucidate the processes that determine the distribution of Nd concentrations and isotopes in an area, which is affected by high atmospheric inputs to the surface ocean, the presence of a vast oxygen

minimum zone (OMZ) at subsurface to intermediate depths and a more restricted deep water circulation than in the western North Atlantic. Furthermore, the data set includes the first high-resolution section across the Canary Islands volcanic archipelago, which enables the investigation of the impact of volcanic island weathering on the otherwise less radiogenic Nd isotope composition of the Atlantic water column.

1.2 General hydrography of the eastern tropical North Atlantic

The study area covers the northwestern African margin from 30° N to the equator, thus including the circulation regimes of the southeastern part of the subtropical gyre and the eastern tropical North Atlantic (Fig.1). The Canary Current (CC) represents the major eastern boundary current of the North Atlantic subtropical gyre and flows southward passing the Gulf of Cadiz and Cape Ghir, where it departs from the margin and feeds into the westbound North Equatorial Current (NEC). In contrast, the thermocline circulation of the tropical eastern Atlantic is dominated by several distinct zonal current bands of relatively small vertical and meridional extent, the occurrence of which is variable in space and time (e.g. Stramma et al., 2005, 2008). The Northern Equatorial Counter Current (NECC) and the Northern Equatorial Undercurrent (NEUC), located at ~3° to 5° N, transport oxygen- and nutrient-rich waters from the western basin into the eastern Atlantic and together with the Guinea Dome (GD) and the NEC in the north contribute to the cyclonic tropical gyre (e.g. Brandt et al., 2010) (Fig. 1). The region between the NEC and the NECC/NEUC represents a shadow zone, which is not ventilated from the north (Luyten and Stommel, 1986). Due to high respiration rates and sluggish ventilation from the south, central and intermediate waters in the region are characterized by hypoxic conditions (Karstensen et al., 2008) (Fig. 2c). The southeastern boundary of the subtropical gyre, called Cape Verde Frontal Zone (CVFZ) represents the boundary between North and South Atlantic Central Waters (Zenk, 1991). Both types of

central waters occupy the layer from below the seasonal thermocline to a density of $\sigma_\theta \approx 27.1$ kg m^{-3} (Stramma et al., 2005) and are characterized by a tight and almost linear θ-S relationship (Harvey, 1982; Tomczak and Hughes, 1980) (Fig. 2). In contrast, South Atlantic Central Water (SACW) is colder and fresher than North Atlantic Central Water (NACW). Surface water in the eastern tropical North Atlantic is called Tropical Surface Water (TSW) and is confined by a sharp thermocline from SACW.

At intermediate depths two water masses prevail: Antarctic Intermediate Water (AAIW) is formed in the frontal system of the Southern Ocean (Talley, 1996) and enters the study area from the south as a tongue of relatively fresh and cold water at depths between 500 and 1200 m (Fig 2b). In contrast, Mediterranean Water (MW) is supplied into the eastern North Atlantic from the Strait of Gibraltar and causes increased salinities, particularly in the depth range from 800 to 1500 m (Hernandez-Guerra et al., 2014).

Underneath, North Atlantic Deep Water (NADW) occupies the water column between 1200 m (1500 m) and the seafloor in the tropics (subtropics). NADW reaches low latitudes with the Deep Western Boundary Current, where it branches off and one part flows along the equator into the eastern basin and continues to flow poleward into both hemispheres, while the remainder continues its southward flow into the Brazil basin (Rhein et al., 1995). Due to admixture of MW, upper NADW (UNADW) within the subtropical area of the section is warmer and more saline than in the tropics. Below a depth of ~3500 m NADW exhibits relatively uniform hydrographic properties, which can be attributed to the restricted inflow of deep waters via the deep fracture zones in the Mid Atlantic Ridge (Schlitzer, 1987; McCartney, 1991) where intense vertical mixing of Antarctic Bottom Water (AABW) with overlying lower NADW (LNADW) (Mercier and Morin, 1997) leads to warmer and more saline bottom waters than in the western Atlantic Basin.

2. Material and Methods

All samples (n=113) were recovered during cruise M81/1 aboard the German research vessel Meteor between February and March 2010. The cruise was officially part of the international GEOTRACES program and corresponds to GEOTRACES cruise GA11.

Our study includes eleven full water column profiles with nine to eleven samples per profile. Station 5 represents a crossover station with the U.S. GEOTRACES cruise GA03 (Stichel et al., 2015), at which the Nd isotope and concentration data were intercalibrated to guarantee comparability of the GEOTRACES Nd isotope and concentration data between different cruises (see supplementary information in Stichel et al., 2015).

2.1 Sampling

The recovery of seawater for the analysis of Nd isotope compositions and concentrations included three different sampling devices. All samples in the depth range from 5 to 5400 m were taken with Niskin bottles attached to a rosette equipped with a standard Seabird SBE-911 plus CTD system. One deep water sample (S11, 5703 m) in the Romanche Fracture Zone was taken with the U.S. GEOTRACES trace metal clean rosette system equipped with Teflon-coated GO-FLO bottles and the same CTD system. In addition, surface seawater samples from depths near 2 m were collected using a towed fish alongside the ship when it was underway to guarantee contamination free sampling. At seven water column profiles the uppermost surface sample was collected using the towed fish shortly before arriving or as soon as possible after leaving the corresponding CTD cast location.

2.2 Analytical treatment

All samples were taken and measured strictly following the recommended GEOTRACES protocols (van de Flierdt et al., 2012). For every sample, 20 l of seawater were collected in

acid-cleaned LDPE collapsible cubitainers. Filtration through 0.45 µm nitrocellulose acetate filters (Milipore) followed sample recovery within two hours. A 2 l aliquot for Nd concentration analysis was separated and the remaining 18 l were used for the determination of the Nd isotope ratios. After filtration all samples were acidified to pH 2 with distilled concentrated hydrochloric acid (1 ml acid per liter of seawater). In order to pre-concentrate Nd in the large volume aliquots, 500 µl of iron-chloride solution (1 g $Fe(III)Cl_3$/ml in 3 M HCl) were added to each sample. After 24 h to equilibrate, precipitation of iron hydroxides was induced by raising the pH to a value of 7.5 – 8.0 using ammonia (Suprapure grade). In a final step the supernatant water was decanted and the settled precipitates were transferred into 2 l wide mouth LDPE bottles for transport to the home laboratory.

At the clean lab facilities of GEOMAR major ions were removed through repeated rinsing of the precipitates with deionized water, subsequently iron was removed applying a liquid-liquid extraction with di-ethyl ether. Neodymium was purified applying an established two-step ion chromatographic column chemistry (Le Fevre and Pin, 2005). In a first column chromatographic step the REEs were separated from other cations using Bio-Rad AG50W-X8 resin (200 – 400 mesh-size, 1.4 ml resin bed). In a second step, Nd was separated from the other REEs using Eichrom Ln Spec resin (50 – 100 µm, 2 ml resin bed).

Neodymium concentrations were obtained applying an isotope dilution method. A defined amount of a $^{150}Nd/^{149}Sm$ spike was added to 0.5 l of the filtered and acidified seawater aliquot and left for equilibration for about 5 days. Subsequently Nd was pre-concentrated using the same iron co-precipitation method. A single column chromatographic separation on Bio-Rad AG50W-X8 was sufficient for preparing the Nd samples for mass spectrometric analysis. A detailed description of the entire analytical procedure is given in Stichel et al. (2012).

All measurements were carried out on a Nu Plasma MC-ICP-MS at GEOMAR. Measured $^{143}Nd/^{144}Nd$ ratios were normalized to $^{146}Nd/^{144}Nd = 0.7219$ to correct for instrumental mass fractionation following an exponential law. A second correction was applied by normalizing all measured $^{143}Nd/^{144}Nd$ ratios to the accepted value of 0.512115 for the JNdi-1 standard (Tanaka et al., 2000), which was repeatedly measured within each session. The external reproducibilities during the different sessions ranged between 0.2 and 0.5 εNd units (2 S.D.). Duplicate measurements of samples resulted in identical $^{143}Nd/^{144}Nd$ ratios within the external standard reproducibility.

3 Results

The εNd signatures in our study area range from -12.9 in NADW at S11 to -8.1 in the mixed layer at S4 (Fig.3a). Nd concentrations (Fig. 3b) range from 11.9 pmol/kg observed within the EUC (S11, 90 m) to 40.2 pmol/kg in AABW at the equator (S11, 5800 m). Dissolved Nd isotope compositions and Nd concentrations as well as corresponding hydrographic parameters are listed in table 1 for each sampling station.

3.1 Nd isotope signatures

A winter mixed layer with salinities above 36.8 reaches down to 70-90 m depth at the subtropical sites (S1 to S5) (Fig. 2b). Near the Canary Islands the isotopic composition of surface (2 – 8 m) and near-surface (~40 m) waters ranges from -9.3±0.5 (S1) to -8.1±0.3 (S4) and shows no vertical variation within the mixed layer (Fig. 3a). The mixed layer at S5 and S6 is less radiogenic and exhibits εNd values between -11.3±0.3 and -10.8±0.3. Pure NACW, identified by its tight θ-S relationship (Fig. 2a), was found at S1 to S5 and reaches down to ~600 m. Its isotopic composition decreases almost linearly with depth from values between -

9.4±0.4 (S1) and -8.4±0.2 (S3) at 100 m to values between -11.4±0.4 (S1) and -10.0±0.3 (S4) at the lower boundary of the water mass.

Tropical Surface Water observed between the Cape Verde Islands and the southern end of the section is characterized by temperatures above 25°C and is confined by a sharp thermocline at a depth between ~30 and 55 m. The Nd isotope composition of TSW ranges between -12.7±0.2 (S7) and -12.0±0.2 (S8). Within the underlying SACW, the isotopic compositions increase from values between -12.5±0.2 (S9) and -11.8±0.4 (S7) at 100 m to values between -12.1±0.2 (S9) and -11.3±0.2 (S10) at 440 to 500 m depth (Fig. 4). Based on its θ-S properties shown in Fig. 2a central water at S6 is a mixture of NACW and SACW with an almost uniform isotopic signature of -11.5±0.3. Comparison to ADCP measurements performed during the entire cruise revealed no clear relationships of the Nd isotope distribution to the current band structures along the section apart from the EUC. The EUC was observed at the equator (S11) with current velocities of ~60 to 80 cm/s between 40 and 100 m depth. Two samples from 70 m and 88 m depth were collected from within the EUC and yielded relatively unradiogenic Nd isotope compositions of -12.8±0.4 and -12.6±0.4, respectively.

The intermediate water layer is characterized by a large N-S gradient in physical properties, reflecting the respective dominance of AAIW at the southern end of the section and of MW near the Canary Islands (Fig. 2a and 2b). The salinity minimum ($S < 35$), associated with the core of AAIW, is most pronounced at the equator and can be followed until ~20°N between 600 and 1200 m depth (Fig. 2b). At the subtropical stations the presence of MW causes increased salinities above 35 between 700 and 1500 m. Despite the large variation in temperature and salinity, isotope signatures of the intermediate layer fall within the rather small range of -12.1±0.2 (S9) to -10.8±0.2 (S11).

In contrast to the low latitude western Atlantic, where the cores of upper and lower NADW are associated with two peaks of the oxygen content (Tsuchiya et al., 1994), the

oxygen concentration of NADW within the eastern basin is vertically uniform but decreases in a northward direction (Fig. 2c). In addition, salinity and temperature of NADW from depths ≤ 2200 m increase northward from about 10°N. Between the equator and 10°N the vertical distribution of both properties is essentially uniform throughout the entire NADW layer. The isotopic composition of UNADW, which occupies the depths between 1200 and 3500 m, ranges from εNd of -12.9±0.4 at 2180 m at the equator (S11) to -10.8±0.3 at 1980 m at S4, located south of the Canary Islands. LNADW yielded isotope signatures between -12.3±0.2 (S10) and -11.3±0.4 (S1). A uniform signature of -12.1±0.4 was observed in the three deepest samples from depths around 4425 m (S5, 7 and 10). The densest water mass of the Atlantic Ocean was only observed within the Romanche Fracture Zone, where a deep thermocline at ~4000 m depth marks the transition from LNADW to AABW. AABW is characterized by salinities below 34.8 and is characterized by Nd isotopic composition between -9.9±0.4 at 4427 m and -9.6±0.3 at 5703 m depth.

3.2. Nd concentrations

Neodymium concentrations in the mixed layer near the Canary Islands are relatively uniform near 21 pmol/kg. Surface water concentrations between 2 and 13°N range between 21.8 (S10) and 27.7 pmol/kg (S9) but, in contrast to the stations around the Canary Islands, decrease rapidly with depth to values around 17 pmol/kg at 40 to 100 m. Lowest Nd concentrations of 12.2 and 11.9 pmol/kg were observed in the EUC (S11) at 70 and 88 m depth, respectively. The distribution of Nd concentrations within the central and intermediate water range differs in close correspondence to the prevailing oxygen levels (Fig. 3). Hypoxic conditions were observed between 6°N and 20°N at depths between ~100 and 800 m. While outside the OMZ Nd concentrations range between 15 and 20 pmol/kg, concentrations within the OMZ are consistently higher than 20 pmol/kg. The concentration maximum of 23.3 pmol/kg was

observed for the sample with a low oxygen concentration of 40.4 µmol/kg (S7). Between 1000 and 2000 m depth Nd concentrations vary little among the water column profiles ranging between 17 and 20 pmol/kg at 1500 and 2000 m depth, respectively. Below 2000 m depth the Nd concentrations increase constantly towards the seafloor. The average rate of increase varies between 1 and 2 pmol/kg per 500 m. The three deepest samples (~4425 m, S5, S7, S10) from the ETNA have a uniform concentration of 27.5 pmol/kg. Highest Nd concentrations of 35.4 to 40.2 pmol/kg were observed in the three AABW samples.

4. Discussion

4.1. Surface waters

The large-scale distribution of neodymium signatures in surface waters between the equator and 30°N agrees well with the data published by Rickli et al. (2010). Swift changes in Nd concentrations and isotopic compositions reflect inputs of radiogenic Nd originating from weathering of the Canary Islands between 25 and 30°N and addition of less radiogenic Nd via partial dissolution of dust particles between 2 and 20°N, as well as effective scavenging and surface water mixing (Rickli et al., 2010). Despite the general agreement in the distribution patterns of Nd isotope and concentration signatures between both data sets, samples collected during winter 2010 (this study) yielded considerably lower concentrations than samples collected in autumn 2005 (Rickli et al., 2010), predominantly in the latitudinal range of the Saharan dust plume (Fig. 5).

Lower Nd concentrations in combination with a maximum surface concentration occurring about 10° further south than in the Rickli et al. (2010) data likely reflect the seasonal variability of the atmospheric dust transport over the eastern tropical North Atlantic, which includes decreasing concentrations from summer to winter (Prospero, 1995), as well as a latitudinal migration from the northernmost position of the dust plume in summer to its southernmost position in winter, which is directly linked to the position of the Intertropical

Convergence Zone (Husar et al., 1997). The monthly average aerosol concentration at 20°W for the 10 months prior to the respective sample collection overlain by surface water concentration shown in Fig. 6 reveals that the surface distribution of Nd is broadly consistent with the aerosol distribution of the respective month of sample collection and the previous months but shows little to no relicts of the respective previous season. The data therefore indicate that dust events cause an instantaneous change of the surface Nd budget by rapidly releasing Nd to the surrounding waters but at the same time scavenge previously present dissolved Nd from the surface layer causing a significant overprint of the existing Nd isotope signature. In addition, it is likely that enhanced biological production during periodic upwelling events intensifies removal of Nd through adsorption onto biogenic particles.

Consistent with the seasonal migration of the ITCZ and associated wind and rainfall patterns the geographical distribution of African dust sources varies on seasonal time scales (Engelstaedter et al., 2006). In order to explain the less radiogenic Nd isotope compositions accompanied by lower Nd concentrations in winter surface waters compared to those found in autumn, contributions from a significantly less radiogenic and possibly less soluble dust source are required. A recent study by Zhao et al. (2018) has shown that even within a particular dust source region and a defined grain size range large variations of up to 7 εNd units can occur. In addition, these authors show that the average Nd isotope composition of potential Northern African (Morocco and Egypt) sources is more radiogenic than the average of sources located in the southern part of Northwest Africa (e.g. Mali, Benin, Togo), which agrees with our observations and the finding that dust sources in the southern Sahel zone are more important for dust supply and composition during the winter season (Engelstaedter et al., 2006). Since no aerosol samples were collected during M81/1 we cannot, however, constrain the origin and composition of the aerosols precisely. Fig. 6 also reveals that so far,

no one has sampled surface waters for Nd isotope and concentration analysis under the highest atmospheric dust loads.

South of the zone of high dust deposition, Nd concentrations decrease rapidly to 15.7 pmol/kg at the equator, which is a consequence of low atmospheric inputs and enhanced scavenging caused by high biogenic particle fluxes near the equator (cf. Voituriez and Herbland, 1981). The EUC flowing eastward at the equator at speeds exceeding 0.8 m/s is characterized by an unradiogenic signature of -12.8±0.4, presumably reflecting unradiogenic contributions to the North Brazil Current originating from the Brazilian shelf region (Jeandel et al., 2005) which are then retroflected and fed into the EUC (Stramma and Schott, 1999). Upwelling of EUC derived waters thus likely also contributes to the unradiogenic surface water Nd isotope compositions at the equator.

Surface waters near the Canary Islands show the most radiogenic Nd isotope signatures in the study area (Fig. 3) and reveal increasingly more radiogenic isotope compositions along the general north-to-south flow direction of the CC (Fig. 1). Compared with nearby open-ocean site USGT10-03 (εNd= -10.9, [Nd]=13 pmol/kg; Stichel et al., 2015) and the assumed precursor signatures in the Gulf of Cadiz (εNd: -10.2 to -9.5, [Nd]=15.6 pmol/kg; Stichel et al., 2015, Dubois-Dauphin et al., 2017, Fig. 1), the elemental Nd concentration at S1 is significantly higher ([Nd]=20.3 pmol/kg) and the isotopic signature is more radiogenic (εNd= -9.3). Thus, we assume that between the Gulf of Cadiz and S1 surface waters receive contributions through the partial dissolution of eolian particles, which increase Nd concentrations on the one hand and mix with more radiogenic waters, which have passed Madeira (εNd = -8.5, Rickli et al., 2010), on the other.

Following the general north-to-south flow direction of the Canary Current through the archipelago, so from station S1 to S4, surface water becomes progressively more radiogenic (εNd: S1: -9.3, S2: -8.4, S3:-8.3, S4: -8.1), but the isotopic change does not include any

significant variation in Nd concentrations ([Nd]=20.7 to 21.0 pmol/kg) thus suggesting control by boundary exchange by the strictest definition (Lacan and Jeandel, 2005). Since the largest shift in εNd occurs from S1 to S2 but the most radiogenic composition is found at station S4 and thus about 400 km to the south of the archipelago and not closest to the volcanic source rocks (S2), we conclude that apart from the "in-situ" occurring isotope exchange between surface waters and sediments deposited along the islands' margins, there has to be a southward advection of suspended lithogenic particles, which continue to contribute to the dissolved Nd budget causing more radiogenic isotope compositions downstream of the archipelago. Although the εNd variations between S2, S3 and S4 are small and mostly overlap within analytical uncertainty, the occurrence of the most radiogenic isotope signatures south of the archipelago is consistent throughout the upper 2000 m.

Near homogenous surface Nd isotope compositions (-11.0) and concentrations (18 pmol/kg) were observed between 20° N and 25° N, a latitudinal range that receives high amounts of dust during the summer season (Fig. 6). Since hydrographic properties show high salinities and low temperatures reflecting a subtropical origin, it is most likely that the observed Nd signatures are set by an interplay of southwestwards advected surface waters from the Canary Islands mixed with less radiogenic and Nd depleted waters from a more offshore located branch of the CC (e.g. USGT10-05, Stichel et al., 2015), complemented by contributions of unradiogenic Nd from Saharan dust inputs.

4.2 Thermocline Waters

The CC transports approximately 4 Sv of NACW southwards through the Canary Islands (Hernandez-Guerra et al., 2005). Near and downstream of the Canary Islands (S1 to S4) the Nd isotopic composition and concentration of upper NACW is high (εNd ≈ -9.2, [Nd]≈ 20.6 pmol/kg) reflecting that inputs and isotopic exchange with the basaltic material from the

volcanic islands not only affect the surface water signature but also the upper Central Water to almost the same degree. At values of εNd = -10.7±1.2 and [Nd]= 18.7±1.6 pmol/kg (n=4, 2SD) the composition of lower NACW (σ_θ: 26.9 to 27.1 kg m^{-3}) closely matches the composition near its site of formation (εNd = -11.5±0.3, Ovide st. 15, Copard et al., 2011) and is thus obviously less affected by the basaltic inputs than upper NACW. Since volume transport of the CC peaks at potential densities around 26.6 kg m^{-3} and decreases with depth (Hernandez-Guerra et al., 2005), we assume that higher current velocities in upper NACW enhance the resuspension of sediments deposited along the flanks of the islands resulting in higher amounts of particles advected in and interacting with upper NACW. In addition, inputs to the surface and their subsequent vertical dispersion as well as the "freshness" of basaltic material introduced along the island's flanks may also contribute to the vertical gradient in the Nd isotope signature of NACW (Fig.7b).

At S5, however, Nd concentrations are lower and isotopic compositions less radiogenic than at closer proximity to the Canary Islands, which is ascribed to mixing between NACW passing through the volcanic archipelago and NACW that had been transported there by more offshore located branches of the CC. However, the trend of decreasing isotopic compositions with depth is maintained. Including previously published NACW data from the eastern (Stichel et al., 2015) and western parts (Lambelet et al., 2016) of the subtropical gyre, it becomes obvious that the above-described trend of decreasing isotopic compositions with depth prevails throughout the entire subtropical gyre (blue symbols in Fig. 7b). Therefore, we conclude that radiogenic contributions from the volcanic islands in the eastern subtropical Atlantic (Azores, Canary Islands, Madeira) and presumably also from some Caribbean Islands are responsible for maintaining the overall relatively radiogenic Nd isotope composition of the near surface subtropical gyre.

In contrast to NACW, the Nd isotope signature of SACW (S7-S11) appears to be predominantly controlled by vertical processes. Similar to the observations made by Stichel et al. (2015) in the OMZ between the Cape Verde Islands and the Mauritanian shelf, Nd concentrations of SACW between 5°N and 13°N correlate well (r^2= 0.75) with prevailing oxygen concentrations and peak at the lower boundary of the water mass, which corresponds to the core of the ETNA's OMZ (σ_θ=27.0 kg m^{-3}) at oxygen concentrations as low as 40 µmol/kg (Fig. 3b, orange symbols in Fig. 7c and 7d).

In contrast to the pronounced and systematic changes in Nd concentrations (between 15.8 to 23.3 pmol/kg) that exist in lower SACW, its isotopic composition is relatively uniform (εNd = -11.6±0.6, n=6, 2SD, Fig. 7b) and does not show any systematic variation between the OMZ and the better ventilated equatorial region. Thus, we assume that the initial isotopic composition of SACW when entering the ETNA is near -11.5 and deviations towards less radiogenic signatures in its upper parts are caused by rapid and continuous isotopic exchange between seawater and sinking particulate material, transferring scavenged unradiogenic Nd from the surface layer (εNd≈ -12.5) to greater depths. Given, however, that the isotopic compositions of adsorbed and released Nd converge with depth, no alteration of the isotopic signature of lower SACW is observed. Assuming that this downward transport of Nd is solely controlled by reversible scavenging (Siddall et al., 2008; Zheng et al., 2016) onto organic material, the remineralization and the consequent release of Nd into the sluggish subsurface water body allows the development of the observed Nd concentration maximum at mid depth.

A further possibility, however, is that SACW present in the ETNA is not significantly influenced by local inputs but that the difference in isotope compositions between its upper and its lower part reflects its heterogenous source regions. According to Stramma and England (1999) the source region of SACW is located in the confluence zone of the Brazil and Falkland Currents, but SACW present in the ETNA contains a large amount of Indian

Central Water transferred into the Atlantic Ocean via Agulhas rings and filaments (Stramma and Schott, 1999 and references therein). Although available data in the latter two regions are sparse, published values by Jeandel (1993) and Garcia-Solsona et al. (2014) from 33°15S, 41°47W and 36.50°S, 13.10°E, respectively, reveal an isotopic range between εNd = -11.8 and -9.2 in water depths between 173 m and 470 m. Overall SACW in the southwestern Atlantic (εNd: -10.0 to -9.2) is apparently more radiogenic than waters of Indian Ocean origin (εNd: -11.8 to -10.7, SW-Indian at S1 in Garcia-Solsona et al. 2014). However, since the average isotope signature of these possible source waters is more radiogenic than SACW present in the ETNA we suggest that the heterogeneous origin of SACW may contribute to the observed vertical gradient but is insufficient to explain the observed Nd isotope distribution without further local (unradiogenic) inputs.

Fig. 7 shows that Central Water present near the CVFZ between 20°N (S6) and 17°N (USGT10-09d – USGT10-11, Stichel et al., 2015) is a mixture of NACW and SACW. Both, hydrographic properties (Fig 7a) as well as their isotopic composition of $-11.73\pm0.23 \leq \varepsilon Nd \leq -10.34\pm0.4$ in the density range of $26.5 \leq \sigma_\theta \leq 27.0$ is intermediate between pure NACW and SACW (Fig.7b) and reflects the confluence and mixing of both water masses at the CVFZ.

4.3 The composition of NADW in the ETNA

The uppermost part of UNADW in the ETNA is truncated by AAIW in the south and by MW in the north, resulting in a high variability of θ-S properties in the depth range between ~1300 and 2000 m (UNADW* in Fig. 8a). The southward decreasing fraction of admixed MW can be tracked by its salinity values at the 2000m depth level (Table 1). Despite MW is characterized by a rather radiogenic isotope signature of εNd= -8.9 (Tachikawa et al., 2004) when entering the eastern Atlantic, the isotopic composition at S1 is almost one εNd unit less radiogenic than at the more southern stations where the fraction of MW is even lower. Similar

to waters below 500 m water depth near the Canary Islands, this is an effect of boundary exchange in its strictest sense with the volcanic island flanks or the seafloor sediments around the archipelago, given that no variation in Nd concentrations is observed.

The sample at 2176 m depth at Station S11 (S=34.96, θ=3.22°C, εNd=-12.9±0.4, [Nd]=17.9 pmol/kg) represents the least altered UNADW composition (see Lambelet et al., 2016) that enters the eastern basin along the equator following southward transport within the DWBC (e.g. Rhein et al., 1995). Between depths of 2200 m and 3500 m UNADW in the ETNA is characterized by a narrowly defined property distribution in θ-S space (green symbols in Fig. 8a) and reflects almost pure UNADW as found in the western North Atlantic. Only near the Canary Islands this layer is also affected by MW leading to slightly increased salinities. Substituting εNd for θ (Fig. 8b) it is obvious that the incorporation of AAIW into the upper parts of UNADW (UNADW*) diminishes rapidly north of the equator and that MW admixture becomes dominant. While the northward increase in θ and S clearly originates from the admixture of MW (cf. Jenkins et al. 2014) the change towards more radiogenic εNd exceeds the expected isotope signature resulting only from mixing of MW and AAIW(indicated by the crossed field confined by the purest UNADW(2176 m, S11), the saltiest UNADW* (1484 m, S1) and the freshest UNADW* (1288 m, S11) in Fig. 8), particularly near the Canary Islands. We attribute these offsets to radiogenic inputs from the Canary and likely from the Cape Verde islands. Again, the lack of any variation in Nd concentrations suggest a predominant control by boundary exchange. In support of this, the Nd isotope compositions of less altered UNADW also reveal an increase of comparable magnitude but at the same time the well-defined θ-S properties rule out that the observed Nd isotope shift is caused by admixture of additional water masses. On average, the isotopic composition of UNADW is -12.4 between the equator and S8 and -11.4 between S1 and S7. Despite showing Nd isotope signatures that are affected by radiogenic inputs to the same

degree, the UNADW layers discussed above show vertical gradients in the distribution of Nd concentrations (Fig. 8c). While the depth range from 1300 m to 2000 m is characterized by a narrow range of Nd concentrations of 17 to 20 pmol/kg that are vertically almost uniform, the layer between 2200 m and 3500 m shows Nd concentrations that increase almost linearly with depth (Fig. 4). This trend is similar to many other deep water profiles in the ocean and continues until the seafloor thus also including the deepest samples from the ETNA. Waters from depths greater than the average crest height of the Mid-Atlantic Ridge (3700 m) are a mixture of LNADW and AABW and are thought to enter the ETNA primarily through the VFZ at 11°N (McCartney et al., 1991). Our samples from this depth range confirm this by showing Nd concentrations essentially indistinguishable from those of deep waters of the Guiana basin in the western North Atlantic (station 30.2 in Lambelet et al., 2016) close the VFZ (purple symbols in Fig. 8b).

The vertical distribution patterns of Nd concentrations in deep waters are similar to those obtained by Stichel et al. (2015) and Lambelet et al. (2016) in the mid-latitude Atlantic. These authors suggested that the rate of lateral mass transport is crucial for the distribution of Nd concentrations in that Nd concentrations are vertically uniform within the fast-flowing water bodies whereas in the underlying layers characterized by lower transport rates dissolution/desorption of previously scavenged Nd increases the concentrations of Nd. However, considering that the accumulated mass transport of NADW in the eastern basin is only a fraction of that transported by the strong DWBC (e.g. Hernandez-Guerra et al., 2014) and highest transport rates in the eastern basin are likely still lower than moderate rates at greater depths (where [Nd] increases) in the western basin, we conclude that differences in volume transport alone cannot lead to the observed distribution patterns of Nd concentrations in the ETNA. Moreover, the vertical distribution of Nd concentrations in deep waters of the (sub)tropical Atlantic is likely also a function of the fraction of AABW contained in deep

waters and thus explains the uniform Nd distribution within the deep low-to-mid latitude North Atlantic (Fig. 8c). In summary, the distribution of Nd isotopes and concentrations in deep waters of the ETNA is mainly set by lateral advection and mixing of water masses characterized by different Nd contents but exchange with the volcanic material changes their isotopic composition between 10°N and 30°N without affecting the Nd concentration of the respective water masses between 1300 and 3500 m. The composition of LNADW is essentially the same as in the western trough of the North Atlantic.

5. Conclusions

We analyzed 113 seawater samples from the eastern tropical North Atlantic for their dissolved Nd concentrations and radiogenic isotope compositions. The data demonstrate the importance of advection and water mass mixing but also of inputs from volcanic islands and Saharan dust. The influence of the volcanic Canary Islands in the eastern (sub)tropical Atlantic is clearly evident in more radiogenic Nd isotope compositions of all water masses from the surface down to a depth of ~3500 m. The shift towards more radiogenic isotope signatures occurs without any significant changes in Nd concentrations. This represents an important example of "boundary exchange" by the strictest definition (Lacan and Jeandel, 2005).

Although the season of maximum dust deposition in the dustiest part of the global ocean was not sampled during our cruise and a previous expedition, the influence of Saharan dust on the Nd isotopic compositions and concentrations is evident in surface and upper central waters. Differences in εNd signatures of the surface ocean between our data and an earlier study that sampled at a different time of the year reveal that different sources of dust influence the surface ocean Nd isotope signature on sub-annual timescales.

In the subsurface waters the OMZ appears to influence the elemental Nd budget in that Nd concentrations of SACW in the OMZ's core are ~5 pmol/kg higher than those of SACW outside the OMZ, which is fully consistent with the results of Stichel et al. (2015). The Nd isotope composition of the OMZ, in contrast, is laterally uniform, suggesting that the isotopic signature of Nd, released through remineralization of organic material in the OMZ, is similar to the original signature of SACW.

The Nd isotope signatures of UNADW reflect its inflow at the equator and admixture of MW north of 10°N but its properties are also modified to some extent by boundary exchange with the volcanic Canary Islands. Only the densest water mass, LNADW, filling the abyssal plains of the eastern basin, appears not to be influenced by the volcanic inputs and shows a Nd isotope signature that is already set by mixing of LNADW and AABW in the western Atlantic basin.

6. Acknowledgements

This work was funded by Deutsche Forschungsgemeinschaft (DFG) grant FR1198/9-1. We thank F/S METEOR crew and scientists of Meteor cruise M81/1 (GEOTRACES cruise GA11) for their help and Jutta Heinze for laboratory support. Finally we would like to thank the two anonymous reviewers for their comments which helped to improve the quality of the manuscript.

7. References

Acker, J. G., Leptoukh, G., 2007. Online Analysis Enhances Use of NASA Earth Science Data, Eos, Trans. AGU, Vol. 88, No. 2, pages 14 and 17.

Albaréde, F., Goldstein, S. L., 1992. World map of Nd isotopes in sea-floor ferromanganese deposits. Geology 20, 761–763.

Arsouze, T., Dutay, J.-C., Lacan, F., Jeandel, C., 2009. Reconstructing the Nd oceanic cycle using a coupled dynamical–biogeochemical model. Biogeosciences 6, 2829–2846.

Bowie, A. R., D. J. Whitworth, E. P. Achterberg, R. F. C. Mantoura, and P. J. Worsfold (2002), Biogeochemistry of Fe and other trace elements (Al, Co, Ni) in the upper Atlantic Ocean, Deep Sea Res., Part I, 49, 605– 636.

Brandt, P., Hormann, V., Körtzinger, A., Visbeck, M., Krahmann, G., Stramma, L., Lumpkin, R., Schmid, C., 2010. Changes in the ventilation of the oxygen minimum zone of the tropical North Atlantic. J. Phys. Oceanogr. 40, 1784–1801.

Copard, K., Colin, C., Frank, N., Jeandel, C., Montero-Serrano, J.-C., Reverdin, G. and Ferron, B., 2011. Nd isotopic composition of water masses and dilution of the Mediterranean outflow along the southwest European margin. Geochem. Geophys. Geosyst. 12, Q06020, http://dx.doi.org/10.1029/2011GC003529.

Dubois-Dauphin, Q., Colin, C., Bonneau, L., Montagna, P., Wu, Q., Van Rooij, D., Reverdin, G., Douville, E., Thil, F., Waldner, A., Frank, N., 2017. Fingerprinting Northeast Atlantic water masses using Neodymium isotopes. Geochim. Cosmochim. Acta 210, 267-288.

Engelstaedter, S., Tegen, I., Washington, R., 2006. North African dust emissions and transport. Earth-Sci. Rev.79, 73–100.

Frank, M., 2002. Radiogenic isotopes: tracers of past ocean circulation and erosional input. Rev. Geophys. 40, 1001, http://dx.doi.org/10.1029/2000RG000094.

Garcia-Solsona, E., Jeandel, C., Labatut, M., Lacan, F., Vance, D., Chavagnac, V. and Pradoux, C., 2014. Rare earth elements and Nd isotopes tracing water mass mixing and particle-seawater interactions in the SE Atlantic. Geochim. Cosmochim. Acta 125, 351–372.

Goldstein, S.L., O'Nions, R.K., Hamilton, P.J., 1984. A Sm–Nd isotopic study of atmospheric dusts and particulates from major river systems. Earth Planet. Sci. Lett.70, 221–236.

Grasse, P., Stichel, T., Stumpf, R., Stramma, L., Frank, M., 2012. The distribution of neodymium isotopes and concentrations in the Eastern Equatorial Pacific: water mass advection versus particle exchange. Earth Planet. Sci. Lett. 353–354, 198–207.

Grasse, P., Bosse, L., Hathorne, E.C., Böning, P., Pahnke, K., and Frank, M., 2017. Short-term variability of dissolved Rare Earth Elements and neodymium isotopes in the entire water column of the Panama Basin. Earth Planet. Sci. Lett. 475, 242-253.

Grousset, F.E., Parra, M., Bory, A., Martinez, P., Bertrand, P., Shimmield, G., Ellam, R.M., 1998. Saharan wind regimes traced by the Sr–Nd isotopic composition of subtropical Atlantic sediments: last glacial maximum vs today. Quat. Sci. Rev.17, 395–409.

Haley B.A., Du, J., Abbott, A.N., McManus, J., 2018. The Impact of Benthic Processes on Rare Earth Element and Neodymium Isotope Distributions in the Oceans. Front. Mar. Sci. 4:426, doi: 10.3389/fmars.2017.00426.

Harvey, J., 1982. θ–S relationships and water masses in the eastern North Atlantic. Deep-Sea Research 29, 1021–1033.

Hernández-Guerra, A., Fraile-Nuez, E., Lopez-Laatzen, F., Martinez, A., Parrilla, G., Velez-Belchi, P., 2005. Canary Current and North Equatorial Current from an inverse box model. Journal of Geophysical Research 110, C12019. http://dx.doi.org/10.1029/2005JC003032.

Hernández-Guerra, A., Pelegrí, J.L., Fraile-Nuez, E., Benítez-Barrios, V., Emelianov, M., Pérez-Hernández, M.D., Vélez-Belchí, P., 2014. Meridional overturning transports at 7.5N and 24.5N in the Atlantic Ocean during 1992–93 and 2010– 11. Progress in Oceanography 128, 98–114.

Howe, J.N.W., Piotrowski, A.M., Hu, R., Bory, A., 2016. Reconstruction of east–west deep water exchange in the low latitude Atlantic Ocean over the past 25,000 years. Earth Planet. 458, 327-336.

Husar, R.B., Prospero, J.M., Stowe, L.L., 1997. Characterization of tropospheric aerosols over the oceans with the NOAA advanced very high resolution radiometer optical thickness operational product. Journal of Geophysical Research, [Atmospheres] 102 (D14), 16,889–16,909.

Jacobsen, S. B., Wasserburg, G. J., 1980. Sm−Nd evolution of chondrites. Earth Planet. Sci. Lett. 50, 139−155.

Jeandel, C., 1993. Concentration and isotopic composition of Nd in the South Atlantic Ocean. Earth Planet. Sci. Lett.117, 581–591.

Jeandel, C., Arsouze, T., Lacan, F., Techine, P. and Dutay, J., 2007. Isotopic Nd compositions and concentrations of the lithogenic inputs into the ocean: a compilation, with an emphasis on the margins. Chem. Geol. 239, 156–164.

Jenkins, W.J., Smethie Jr., W.M., Boyle, E.A., Cutter, G.A., 2014. Water mass analysis for the U.S. GEOTRACES (GA03) North Atlantic sections. Deep-Sea Res. II.

Karstensen, J., Stramma, L., and Visbeck, M., 2008. Oxygen minimum zones in the eastern tropical Atlantic and Pacific oceans, Prog. Oceanogr. 77, 331–350.

Johannesson, K.H., Burdige, D.J., 2007. Balancing the global oceanic neodymium budget: evaluating the role of groundwater. Earth Planet. Sci. Lett.253, 129–142.

Lacan, F., Jeandel, C., 2004. Neodymium isotopic composition and rare earth element concentrations in the deep and intermediate Nordic Seas: constraints on the Iceland Scotland Overflow Water signature. Geochem. Geophys. Geosyst.5, Q11006. http://dx.doi.org/10.1029/2004GC000742.

Lacan, F., Jeandel, C., 2005. Neodymium isotopes as a new tool for quantifying exchange fluxes at the continent–ocean interface. Earth Planet. Sci. Lett. 232, 245–257.

Lambelet, M., van de Flierdt, T., Crocket, K., Rehkämper, M., Kreissig, K., Coles, B., Rijkenberg, M.J.A., Gerringa, L.J.A., de Baar, H.J.W., Steinfeldt, R., 2016. Neodymium

isotopic composition and concentration in the western North Atlantic Ocean: Results from the GEOTRACES GA02 section. Geochim. Cosmochim. Acta 177, 1–29.

Luyten, J. R., Stommel, H., 1986. Gyres driven by combined wind and buoyancy flux, J. Phys. Oceanogr., 16, 1551–1560.

Machín, F., Hernández-Guerra, A., Pelegrí, J.L., 2006. Mass fluxes in the Canary Basin. Progress in Oceanography 70, 416–447.

McCartney, M., Bennett, S., Woodgate-Jones, M., 1991. Eastward flow through the Mid-Atlantic Ridge at 11N and its influence on the abyss of the eastern basin. Journal of Physical Oceanography 21, 1089–1121.

McCartney, M.S., Curry, R.A., 1993. Transequatorial flow of Antarctic Bottom Water in the western Atlantic Ocean: Abyssal geostrophy at the equator. J. Phys. Oceanogr. 23, 1264-1276.

Mercier, H., Morin, P., 1997. Hydrography of the romanche and chain fracture zones. J. Geophys. Res. 102, 10373–10389.

Molina-Kescher, M., Hathorne, E.C., Osborne, A.H., Behrens, M.K., Kölling, M., Pahnke, K., and Frank, M., 2018. The influence of basaltic islands on the oceanic REE distribution: A case study from the tropical South Pacific. Front. Mar. Sci. 5:50, doi:10.3389/fmars.2018.00050.

Piepgras, D.J., Wasserburg, G.J., 1987. Rare earth element transport in the western North Atlantic inferred from Nd isotopic observations. Geochim. Cosmochim. Acta51, 1257–1271.

Piepgras, D.J., Wasserburg, G.J., 1980. Nd isotopic variations in seawater, Earth Planet. Sci. Lett. 50, 128-138.

Poehle, S., Koschinsky, A., 2017. Depth distribution of Zr and Nb in seawater: The potential role of colloids or organic complexation to explain non-scavenging-type behavior. Mar. Chem. 188, 18-32.

Prospero, J.M., 1995. The Atmospheric transport of particles to the ocean, in: Particle Flux in the Ocean (Eds. V. Ittekkot et al.), John Wiley & Sons, New York, 19-52.

Rempfer, J., Stocker, T.F., Joos, F., Dutay, J.-C., Siddall, M., 2011. Modelling Nd-isotopes with a coarse resolution ocean circulation model: sensitivities to model parameters and source/sink distributions. Geochim. Cosmochim. Acta75, 5927–5950.

Rhein, M., Stramma, L., Send, U., 1995. The Atlantic Deep Western Boundary Current: water masses and transports near the equator. J. Geophys. Res. 100, 2441-2457.

Rickli, J., Frank, M., Halliday, A.N., 2009. The hafnium–neodymium isotopic composition of Atlantic seawater. Earth Planet. Sci. Lett.280, 118–127.

Rickli, J., Frank, M., Baker, A.R., Aciego, S., de Souza, G., Georg, R.B., Halliday, A.N., 2010. Hafnium and neodymium isotopes in surface waters of the eastern Atlantic Ocean:

implications for sources and inputs of trace metals to the ocean. Geochim. Cosmochim. Acta74, 540–557.

Schlitzer, R., 1987. Renewal rates of east Atlantic Deep Water estimated by inversion of ^{14}C data. J. Geophys. Res., 92, 2953-2969.

Schlitzer R., 2012. Ocean Data View. http://odv.awi.de.
Schmitz, W.J., Jr. and McCartney, M.S., 1993. On the North Atlantic circulation. Reviews of Geophysics 31, 29-49.

Stichel, T., Frank, M., Rickli, J., Haley, B.A., 2012. The hafnium and neodymium isotope composition of seawater in the Atlantic sector of the Southern Ocean. Earth Planet. Sci. Lett.317–318, 282–294.

Stichel, T., Hartman, A.E., Duggan, B., Goldstein, S.L., Scher, H., Pahnke, K., 2015. Separating biogeochemical cycling of neodymium from water mass mixing in the Eastern North Atlantic. Earth Planet. Sci. Lett. 412, 245–260.

Stramma, L., England, M., 1999. On the water masses and mean circulation of the South Atlantic Ocean. Journal of Geophysical Research, 104, 20,863-20,883.

Stramma, L., Schott, F., 1999. The mean flow field of the tropical Atlantic Ocean. Deep-Sea Res., Part 2, Top. Stud. Oceanogr.46, 279–303.

Stramma, L., Hüttl, S., Schafstall, J., 2005. Water masses and currents in the upper tropical northeast Atlantic off northwest Africa. J. Geophys. Res.110, C12006, http://dx.doi.org/10.1029/2005JC002939.

Stramma, L., Brandt, P., Schafstall, J., Schott, F., Fischer, J., and Körtzinger, A., 2008. Oxygen minimum zone in the North Atlantic south and east of the Cape Verde Islands, J. Geophys. Res. Oceans 113, C04014, doi:10.1029/2007jc004369.

Tachikawa, K., Jeandel, C., Roy-Barman, M., 1999. A new approach to the Nd residence time in the ocean: the role of atmospheric inputs. Earth Planet. Sci. Lett.170, 433–446.

Tachikawa, K., Roy-Barman, M., Michard, A., Thouron, D., Yeghicheyan, D., Jeandel, C., 2004. Neodymium isotopes in the Mediterranean Sea: comparison between sea-water and sediment signals. Geochim. Cosmochim. Acta68, 3095–3106. http://dx.doi.org/10.1016/j.gca.2004.01.024.

Talley, L.D., 1996. Antarctic intermediate water in the South Atlantic. In: Wefer, G., Berger, W.H., Siedler, G., Webb, D.J. (Eds.), The South Atlantic - Present and Past Circulation, Springer, Berlin, pp. 219-238.

Tanaka, T., Togashi, S., Kamioka, H., Amakawa, H., Kagami, H., Hamamoto, T., Yuhara, M., Orihashi, Y., Yoneda, S., Shimizu, H., Kunimaru, T., Takahashi, K., Yanagi, T., Nakano, T., Fujimaki, H., Shinjo, R., Asahara, Y., Tanimizu, M., Dragusanu, C., 2000. JNdi-1: a neodymium isotopic reference in consistency with LaJolla neodymium. Chem. Geol.168, 279–281.

Tomczak, M., Hughes, P., 1980. Three dimensional variability of water masses and currents in the Canary Current upwelling region. “Meteor“ Forschungs-Ergebnisse A 21, 1–24.

Tsuchiya, M., Talley, L.D., McCartney, M.S., 1994. Water-mass distributions in the western South Atlantic; A section from South Georgia Island (54S) northward across the equator, J. Mar. Res., 52, 55-81.

van de Flierdt T., Pahnke K., Amakawa H., Andersson P., Basak C., Coles B., Colin C., Crocket K., Frank M., Frank N., Goldstein S. L., Goswami V., Haley B. A., Hathorne E. C., Hemming S. R., Henderson G. M., Jeandel C., Jones K., Kreissig K., Lacan F., Lambelet M., Martin E. E., Newkirk D. R., Obata H., Pena L., Piotrowski A. M., Pradoux C., Scher H. D., Schöberg H., Singh S. K., Stichel T., Tazoe H., Vance D., Yang, J., 2012. GEOTRACES intercalibration of neodymium isotopes and rare earth element concentrations in seawater and suspended particles. Part 1: reproducibility of results for the international intercomparison. Limnol. Oceanogr. Methods 10, 234–251.

von Blanckenburg, F., 1999 Tracing Past Ocean Circulation, Science 286, 1862–1863.

Voituirez, B., Herbland, A., 1981 Primary production in the tropical Atlantic Ocean mapped from the oxygen values of Equalant I and II (1963). Bulletin of Marine Science, 31,853-863.

Zenk, W., Klein, B., Schröder, M., 1991. Cape Verde frontal zone. Deep-Sea Research 38, 505–530.

Zhao, W., Balsam, W., Williams, E., Long, X., Ji, J., 2018. Sr–Nd–Hf isotopic fingerprinting of transatlantic dust derived from North Africa. Earth and Planet. Sci. Lett. 486, 23–31.

Zheng, X., Plancherel, Y., Saito, M.A., Scott, P.M., Henderson, G.M., 2016. Rare earth elements (REEs) in the tropical South Atlantic and quantitative deconvolution of their non-conservative behaviour. Geochim. Cosmochim. Acta 177, 217-237.

Table 1: Sample locations and depths, hydrographic properties, Nd isotope compositions and Nd concentrations for the 11 water column stations collected during GEOTRACES cruise GA11

	depth (m)	pot. temp. (°C)	Salinity	pot. dens. (kg/m^3)	Oxygen (µmol/kg)	$^{143}Nd/^{144}Nd^*$	$\varepsilon Nd^{\#}$	External reproducibility (2 S.D.)	[Nd] (pmol/kg)
S1	**28° 59.64' N**	**15° 20.53' W**	**3598m**						
110-1	8	20.22	36.87	26.14	227.12	0.512162	-9.3	0.5	20.7
110-1	38	20.09	36.87	26.17	228.05	0.512178	-9.0	0.4	20.5
110-1	100	19.41	36.79	26.29	224.39	0.512154	-9.4	0.4	20.8
107-1	197	16.6	36.42	26.70	211.88	0.512093	-10.6	0.5	21.9
107-1	497	11.95	35.66	27.12	184.16	0.512055	-11.4	0.4	19.8
107-1	893	8.85	35.44	27.49	159.36	0.512058	-11.3	0.5	19.1
107-1	1484	6.36	35.39	27.82	208.11	0.512036	-11.7	0.4	17.5
107-1	1977	4.42	35.16	27.87	231.46	0.512030	-11.9	0.4	18.0
107-1	2467	3.15	35.01	27.88	239.42	0.512054	-11.4	0.5	19.0
107-1	3447	2.26	34.92	27.89	244.75	0.512060	-11.3	0.4	21.2
S2	**28° 3.77' N**	**16° 3.10' W**	**2047m**						
117-1	2	19.4	36.94			0.512205	-8.4	0.3	20.7
115-1	39	20.32	36.89	26.12	227.61	0.512204	-8.5	0.2	22.1
115-1	97	20.28	36.88	26.13	226.74	0.512193	-8.7	0.2	22.3
115-1	297	15.19	36.16	26.83	197.62	0.512140	-9.7	0.2	18.6
115-1	495	12.35	35.7	27.07	173.59	0.512074	-11.0	0.2	18.5
113-1	755	9.75	35.42	27.33	147.25	0.512083	-10.8	0.2	18.3
113-1	891	8.61	35.36	27.47	152.14	0.512070	-11.1	0.2	17.4
113-1	1189	7.32	35.36	27.66	175.05	0.512059	-11.3	0.2	16.8
113-1	1567	5.38	35.24	27.83	212.71	0.512048	-11.5	0.2	17.2
113-1	1984	4.04	35.1	27.87	229.65	0.512074	-11.0	0.3	17.5
S3	**27° 12.04' N**	**17° 0.03' W**	**3619m**						
121-1	5	20.77	36.92	26.02	226.98	0.512211	-8.3	0.2	20.7
121-1	40	20.76	36.92	26.03	227.11	0.512201	-8.5	0.2	20.8
121-1	99	18.28	36.63	26.45	210.86	0.512206	-8.4	0.2	19.3
119-1	349	13.43	35.86	26.97	190.93	0.512098	-10.5	0.2	18.1
119-1	735	8.9	35.29	27.37	129.48	0.512074	-11.0	0.2	19.2
119-1	993	7.07	35.18	27.56	149.26	0.512079	-10.9	0.2	17.8
119-1	1487	5.65	35.24	27.79	201.49	0.512078	-10.9	0.3	17.1
119-1	1981	3.96	35.08	27.86	225	0.512079	-10.9	0.3	17.4
119-1	2471	3.13	34.99	27.87	232.19	0.512060	-11.3	0.3	19.5
119-1	3446	2.25	34.92	27.89	237.6	0.512058	-11.3	0.3	20.5
S4	**25° 32.73' N**	**17° 31.20' W**	**3204m**						
126-1	6	21.63	37	25.84	223.48	0.512222	-8.1	0.3	21.0
126-1	41	21.5	36.98	25.87	223.64	0.512221	-8.1	0.3	20.9
126-1	100	20.99	36.91	25.95	222.7	0.512202	-8.5	0.3	20.5
125-1	349	14.44	36.03	26.87	192.31	0.512123	-10.0	0.3	18.4
125-1	744	8.39	35.15	27.34	104.57	0.512075	-11.0	0.3	19.1
125-1	1000	7.55	35.24	27.53	149.39	0.512080	-10.9	0.3	26.2
125-1	1485	5.37	35.19	27.78	200.1	0.512070	-11.1	0.3	16.9
125-1	1979	3.99	35.08	27.85	224.95	0.512083	-10.8	0.3	17.4
125-1	2469	3.07	34.99	27.88	233.73	0.512054	-11.4	0.3	18.3
125-1	3055	2.44	34.93	27.89	236.82	0.512052	-11.4	0.3	28.8
S5	**24° 0.00' N**	**22° 0.06' W**	**4611m**						
130-1	6	22.41	37.09	25.70	220.53	0.512075	-11.0	0.3	18.3
130-1	40	22.36	37.09	25.71	220.23	0.512058	-11.3	0.3	17.3
130-1	100	19.63	36.79	26.23	199.5	0.512092	-10.7	0.3	15.7

130-1	348	14.17	35.95	26.89	162.92	0.512095	-10.6	0.3	19.0
130-1	496	11.88	35.61	27.09	138.85	0.512044	-11.6	0.3	18.9
128-1	740	9	35.29	27.35	128.27	0.512034	-11.8	0.3	19.3
128-1	1486	5.19	35.17	27.80	204.66	0.512057	-11.3	0.3	18.1
128-1	1978	3.8	35.06	27.86	227.57	0.512028	-11.9	0.3	17.5
128-1	2958	2.55	34.95	27.89	248.63	0.512017	-12.1	0.3	20.0
128-1	4425	1.97	34.89	27.90	253	0.512018	-12.1	0.3	27.6
S6	**19° 25.25' N**	**20° 26.53' W**	**3424m**						
138-1	5	22.48	36.71	25.38	220.47	0.512086	-10.8	0.3	18.2
138-1	41	22.4	36.71	25.40	220.37	0.512065	-11.2	0.3	18.2
136-1	99	20.9	36.63	25.77	181.58	0.512066	-11.2	0.3	17.3
136-1	328	12.53	35.51	26.88	57.26	0.512047	-11.5	0.3	21.3
136-1	745	7.95	35.03	27.31	85.98	0.512051	-11.5	0.3	21.2
136-1	994	6.53	34.98	27.47	123.26	0.512048	-11.5	0.3	19.0
136-1	1486	4.62	35.03	27.74	194.58	0.512027	-11.9	0.3	18.6
136-1	1977	3.56	35	27.83	227.97	0.512049	-11.5	0.3	18.7
136-1	3157	2.41	34.93	27.89	244.58	0.512040	-11.7	0.3	21.5
S7	**12° 58.61' N**	**20° 19.99' W**	**4678m**						
147-1	2	25.67	35.48			0.511988	-12.7	0.2	25.9
145-1	40	22.74	35.9	24.69	197.9	0.512028	-11.9	0.4	17.8
145-1	99	14.71	35.5	26.43	83.88	0.512034	-11.8	0.4	16.8
145-1	298	11.4	35.19	26.86	67.23	0.512061	-11.3	0.4	20.4
145-1	437	10.15	35.14	27.04	40.44	0.512051	-11.5	0.4	23.3
142-1	695	7.71	34.96	27.29	76.08	0.512075	-11.0	0.4	22.2
142-1	1387	4.47	34.98	27.72	192.87	0.512048	-11.5	0.4	19.9
140-1	1978	3.35	34.97	27.83	235.5	0.512024	-12.0	0.4	19.5
140-1	2961	2.45	34.93	27.88	246.38	0.512041	-11.6	0.4	23.7
140-1	4426	1.88	34.88	27.89	245.92	0.512023	-12.0	0.4	28.1
S8	**9° 30.00' N**	**20° 20.00' W**	**4276m**						
154-1	2	27.95	35.45			0.512023	-12.0	0.2	25.3
152-1	100	14.53	35.49	26.46	107.45	0.512000	-12.4	0.3	16.0
152-1	199	12.74	35.27	26.66	100.25	0.512034	-11.8	0.3	16.6
152-1	428	10.45	35.16	27.01	39.81	0.512054	-11.4	0.3	22.3
150-1	795	6.29	34.77	27.34	91.88	0.512074	-11.0	0.3	25.1
150-1	1488	4.09	34.94	27.73	210.73	0.512012	-12.2	0.3	19.6
150-1	1979	3.27	34.95	27.83	242.23	0.512022	-12.0	0.3	19.0
148-1	2470	2.8	34.94	27.86	247.11	0.512009	-12.3	0.3	22.4
148-1	2961	2.43	34.92	27.88	249.54	0.512003	-12.4	0.3	21.7
148-1	4037	1.98	34.89	27.89	249.63	0.512006	-12.3	0.3	26.2
S9	**5° 59.99' N**	**20° 20.00' W**	**2754m**						
160-1	2	29.05	35.33			0.511996	-12.5	0.3	27.7
158-1	40	26.53	36	23.62	202.62	0.512044	-11.6	0.2	16.7
158-1	99	15.57	35.61	26.32	100.83	0.511996	-12.5	0.2	16.8
155-1	200	13.15	35.31	26.61	80.44	0.511995	-12.5	0.2	18.2
155-1	497	7.84	34.77	27.12	74.63	0.512018	-12.1	0.2	21.3
155-1	745	5.75	34.62	27.29	99.99	0.512018	-12.1	0.2	19.7
155-1	1486	4.09	34.94	27.74	217.75	0.511994	-12.6	0.2	18.3
155-1	1978	3.31	34.96	27.82	242.47	0.511986	-12.7	0.2	18.2
155-1	2272	2.99	34.95	27.85	246.39	0.511986	-12.7	0.2	19.1
155-1	2668	2.62	34.93	27.87	247.54	0.511993	-12.6	0.2	20.0
S10	**2° 8.98' N**	**20° 12.40' W**	**4594m**						
160-1	2	28.94	35.72			0.512017	-12.1	0.3	21.8
163-1	40	27.99	35.91	23.09	206.36	0.512021	-12.0	0.2	18.0
163-1	100	15.44	35.62	26.36	114.39	0.512013	-12.2	0.2	14.4
163-1	342	9.25	34.86	26.97	108.89	0.512036	-11.7	0.2	21.2
163-1	498	7.25	34.64	27.10	132.13	0.512058	-11.3	0.2	15.8
161-1	792	4.91	34.56	27.34	144.11	0.512058	-11.3	0.2	17.4

161-1	1485	4.16	34.94	27.73	220.56	0.511999	-12.5	0.2	18.7
161-1	2471	2.8	34.94	27.86	250.25	0.512008	-12.3	0.2	20.6
161-1	3450	2.19	34.9	27.88	250.35	0.512011	-12.2	0.2	23.3
161-1	4426	1.87	34.88	27.89	252.55	0.512018	-12.1	0.2	27.2
S11	**0° 36.91' S**	**20° 2.55' W**	**6642m**						
166-1	2	28.26	35.58			0.512001	-12.4	0.3	15.7
175-1	70	22.81	36.39	25.05	190.12	0.511984	-12.8	0.4	12.2
173-1	88	18.12	35.95	25.98	169.47	0.511991	-12.6	0.4	11.9
173-1	328	9.63	34.89	26.93	105.28	0.512054	-11.4	0.4	16.2
171-1	694	5.11	34.5	27.27	154.6	0.512085	-10.8	0.4	16.8
169-1	1288	4.41	34.9	27.66	203.64	0.512049	-11.5	0.4	20.2
169-1	2176	3.23	34.96	27.84	254.63	0.511978	-12.9	0.4	17.9
169-1	3626	2.11	34.9	27.89	261.54	0.512040	-11.7	0.4	24.2
167-1	4427	0.88	34.78	27.88	239.69	0.512130	-9.9	0.4	35.4
167-1	5108	0.69	34.76	27.88	238.06	0.512142	-9.7	0.4	37.4
170-1	5703	0.67	34.75	27.88	218.34	0.512147	-9.6	0.4	40.2
additional surface water samples									
SF02	**21° 45.41' N**	**21° 13.81' W**							
135-1	2	21.6	36.9			0.512078	-10.9	0.3	18.1
SF03	**19° 33.88' N**	**20° 29.41' W**							
135-1	2	22.81	36.71			0.512078	-10.9	0.3	17.0
SF04	**2° 50.71' N**	**20° 20.00' W**							
160-1	2	27.4	35.69			0.512018	-12.1	0.3	27.2

* Normalised relative to JNdi value of 0.512115 (Tanaka et al., 2000)

εNd values were calculated relative to a CHUR of 0.512638 (Jacobsen and Wasserburg, 1980)

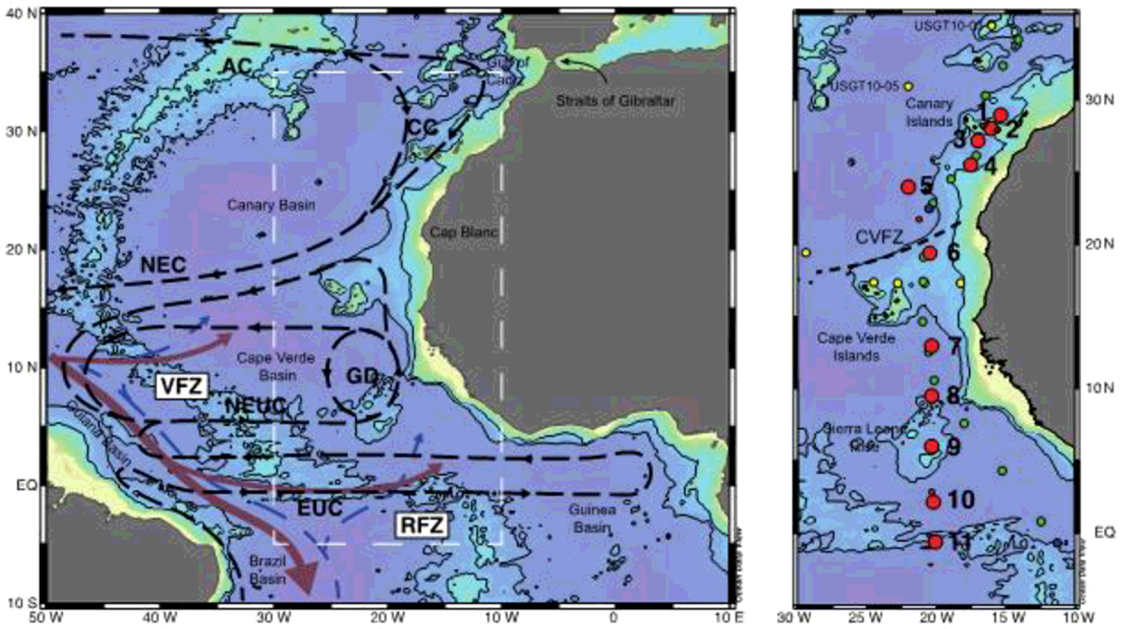

Figure 1: Map of the tropical North Atlantic Ocean. Black dashed lines indicate the schematic circulation of the upper ocean, including the Azores Current (AC), the Canary Current (CC), the North Equatorial Current (NEC), the Guinea Dome (GD), the North Equatorial Undercurrent (NEUC) and the Equatorial Undercurrent (EUC). Red arrows indicate the flow paths of NADW, while dashed blue arrows represent the flow path of AABW across the Romanche and Vema Fracture Zones (RFZ and VFZ) into the eastern basin. The white dashed line marks the inset shown on the right, including the locations of seawater profiles of cruise GA11 presented in this study (red circles with numbers), two additional surface water samples (smaller red circles), surface water samples of Rickli et al. (2010, green circles), seawater profiles from Rickli et al. (2009, blue circles) and seawater profiles of Stichel et al. (2015, yellow circles). A dashed black line shows the location of the Cape Verde Frontal Zone (CVFZ). The map was created with the ODV Software (Schlitzer, 2012)

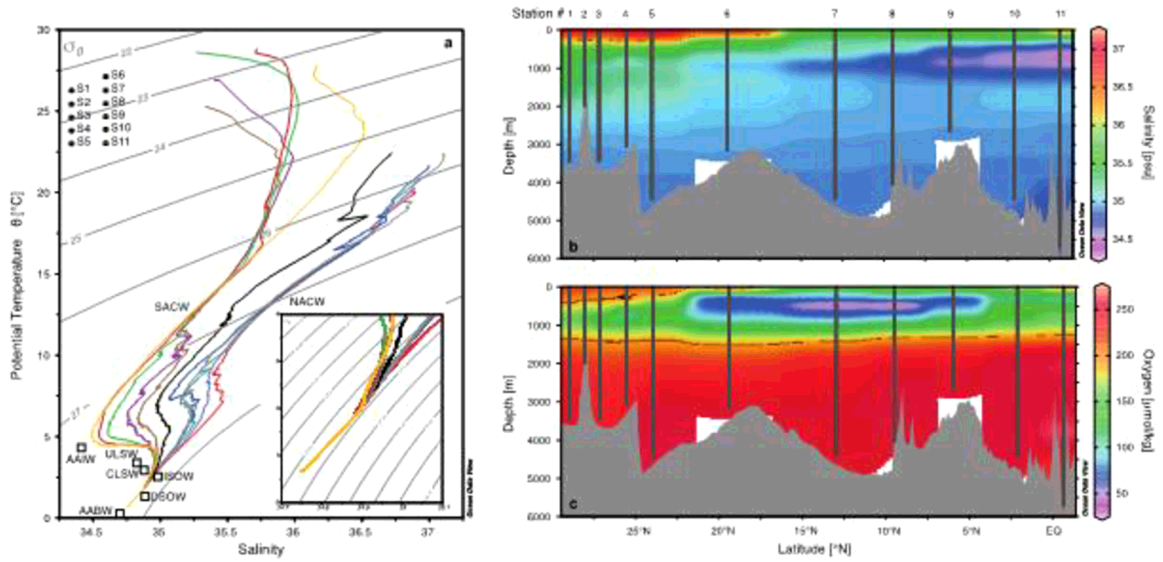

Figure 2: Salinity versus potential temperature of all seawater profiles of this study (a). Water mass endmember compositions following Jenkins et al. (2015) and references therein are indicated by black squares with abbreviations as follows: AABW: Antarctic Bottom Water, AAIW: Antarctic Intermediate Water, CLSW: Classic Labrador Seawater, DSOW: Denmark Straight Overflow Water, ISOW: Iceland Scotland Overflow Water, NACW: North Atlantic Central Water, SACW: South Atlantic Central Water, TSW: Tropical Surface Water, ULSW: Upper Labrador Seawater. Sections of salinity (b) and oxygen (c) distribution from the equator to 35°N. Grey vertical lines represent the locations of the CTD casts with associated station numbers above. This figure was created with the ODV Software (Schlitzer, 2012)

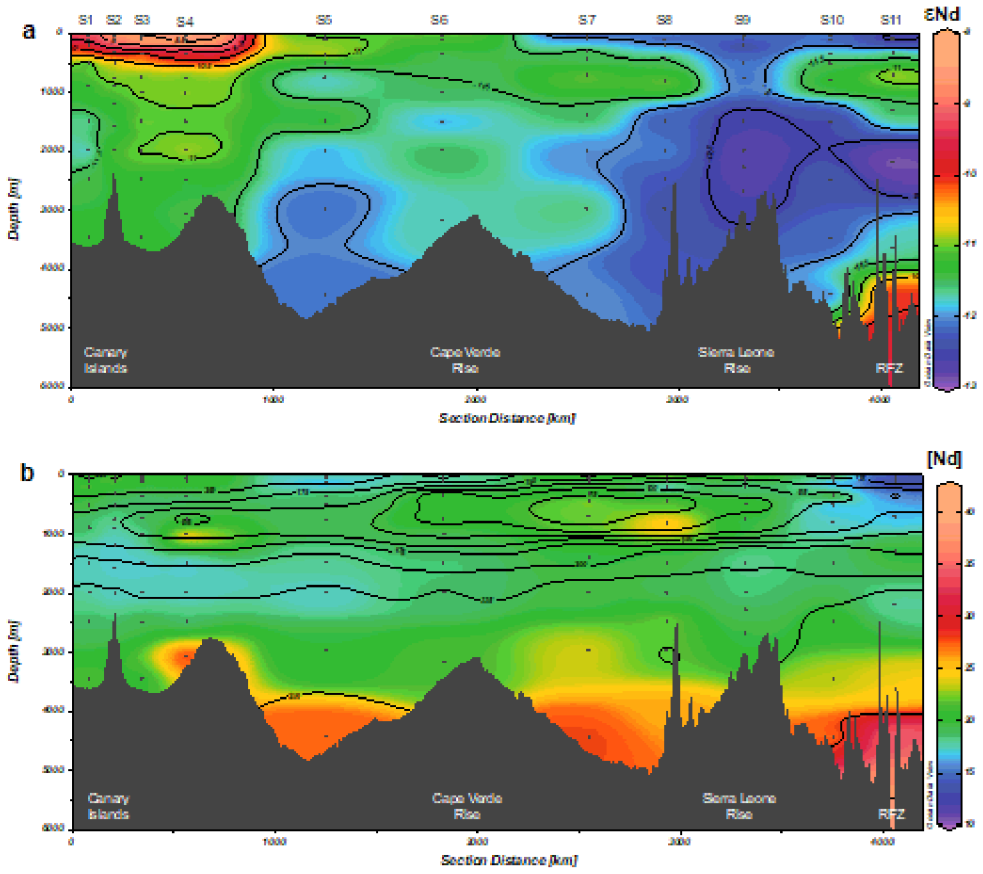

Figure 3: Sections of εNd (upper panel) and Nd concentrations (lower panel) for the eastern Atlantic from 30°N to the Romanche Fracture Zone. Sections include isolines for εNd in the upper panel and for oxygen concentrations (µmol/kg) in the lower panel. Plots were created with the ODV Software (Schlitzer, 2012)

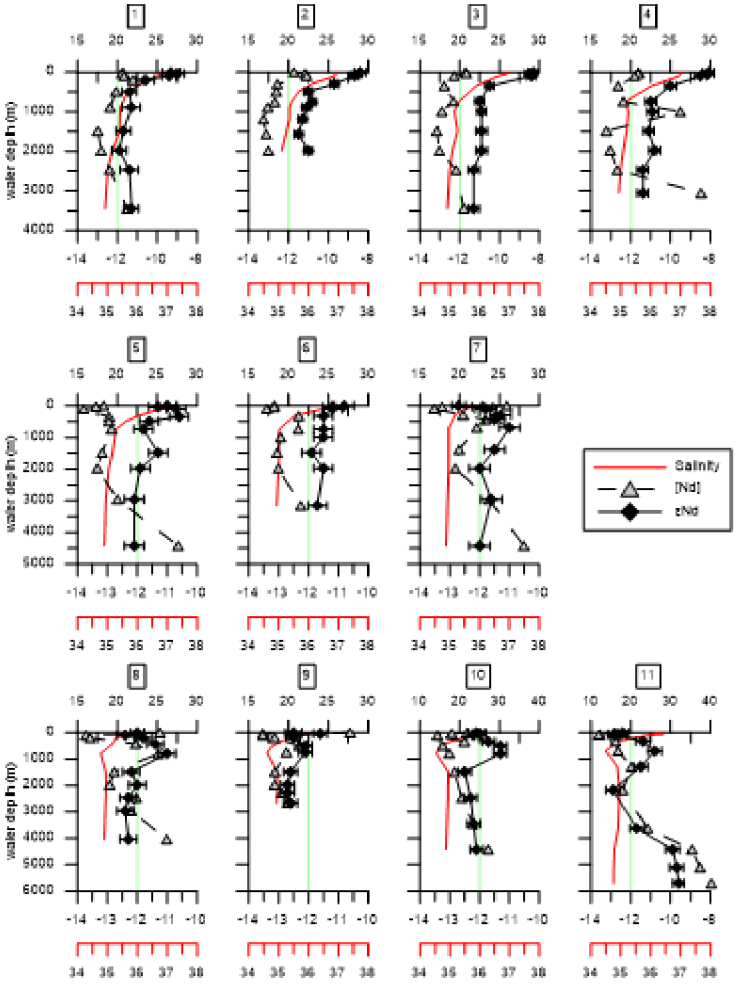

Figure 4: Nd concentrations, isotopic compositions and salinity for each water column profile. The vertical green line indicates an isotopic composition of εNd = -12 and serves as a visual aid for comparison. Note that scales may vary.

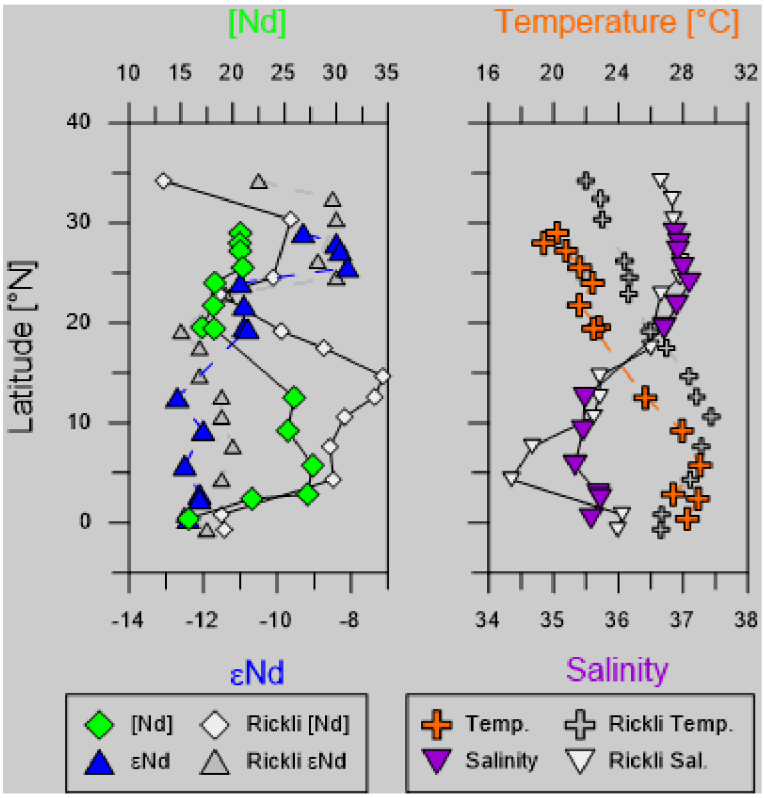

Figure 5: Neodymium concentrations and isotopic compositions of surface water (left) and corresponding temperatures and salinities (right) plotted against latitude. Coloured symbols are used for new data of this study, while grey symbols are used for data by Rickli et al. (2010). Sampling locations are also shown in Fig. 1.

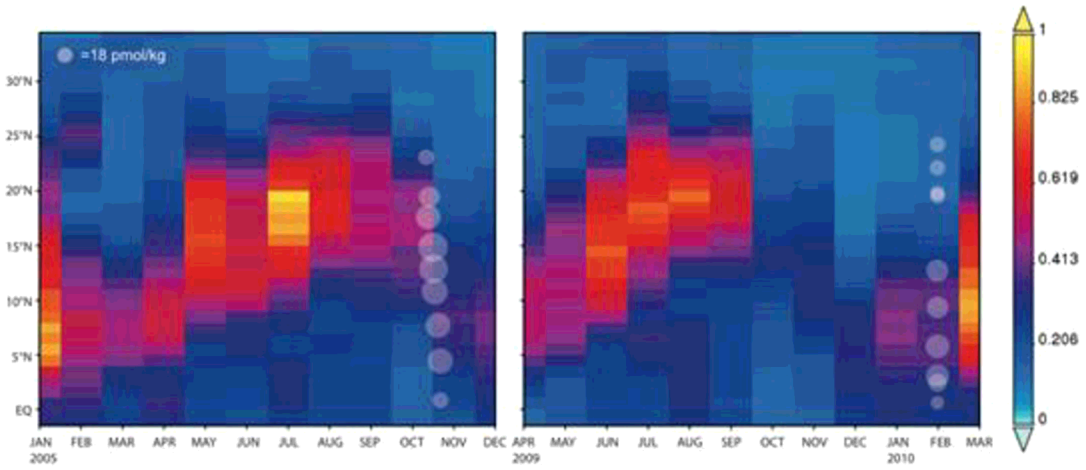

Figure 6: Monthly averaged aerosol optical depth (AOD) over 20°W for January to December 2005 (left) and for April 2009 to March 2010 (right) with surface water Nd concentrations plotted on top, which were collected along or close to 20°W. Circle sizes correspond to Nd concentrations. Analyses and visualizations used in this paper were produced with the Giovanni online data system, developed and maintained by the NASA GES DISC.

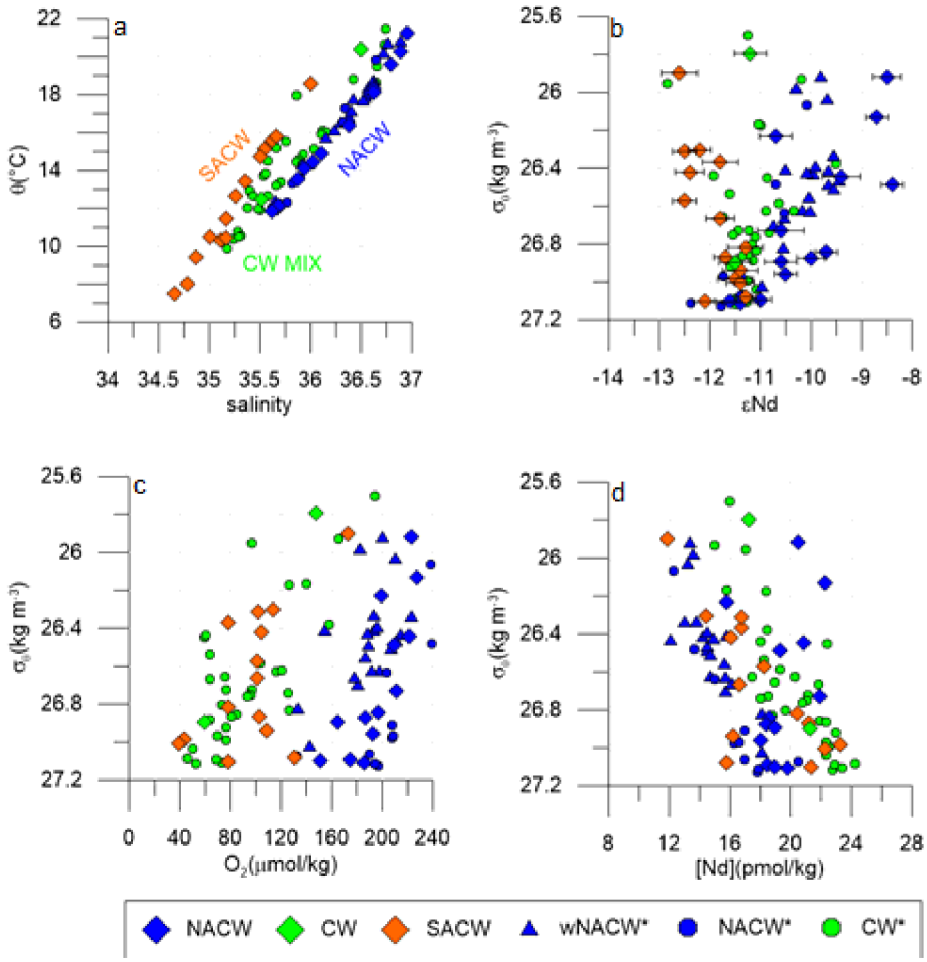

Figure 7: Potential temperature versus salinity (a) and potential density (σ_θ) versus Nd isotope composition (b),oxygen concentration (c), and Nd concentration (d). Data of this study are marked by large diamonds (blue for NACW, orange for SACW, green for CW (mix of SACW and NACW near the CVFZ)). Literature data are indicated by small blue circles for NACW (data from stations US-GT10-01 to 10-05 (Stichel et al., 2015)), blue triangles for western NACW (wNACW, station 15.6 to 30.2 (Lambelet et al., 2016)) and green circles for CW* (data from stations US-GT10-09 to 10-11 (Stichel et al., 2015)).

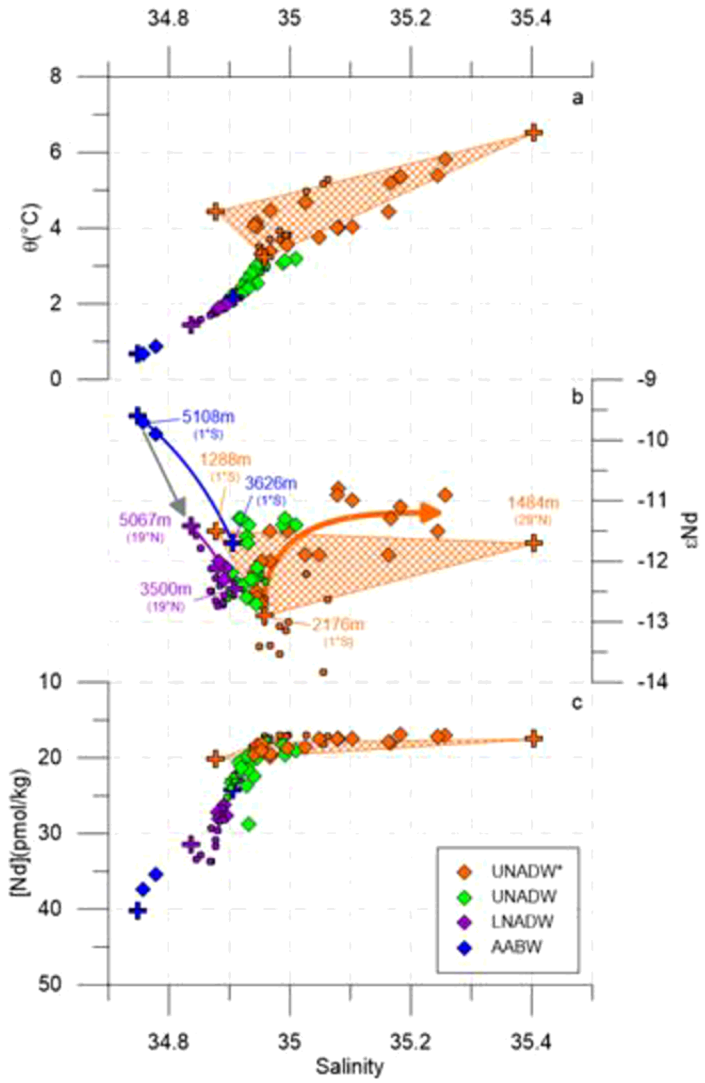

Figure 8: Potential temperature θ (a), neodymium isotope composition εNd (b) and neodymium concentration [Nd] (c) versus salinity of all water samples from depths exceeding 1200 m. Subdivision as follows: UNADW*: 1200 – 2000 m (orange), influenced by AAIW and MW; UNADW: 2000 – 3500 m (green); LNADW: 3500 – 4500 m (purple); AABW: 4400 – 5703 m at S11 (blue). Western North Atlantic deep water data from station 15.6 to station 30.2 from Lambelet et al. (2016) are included as small circles with the same subdivision. The orange crossed area marks the property field confined by the freshest AAIW-influenced UNADW (S11, 1288 m), the saltiest MW-influenced UNADW (S1, 1484 m) and the purest UNADW (S11, 2176 m). The orange arrow in (b) illustrates the northward

evolution of UNADW*. Mixing lines between LNADW and AABW of the RFZ (S11) and VFZ (St. 30.2) are shown in blue and purple, respectively. The grey arrow in (b) highlights the property changes of AABW across the equator.